New Journal of Physics
The open access journal at the forefront of physics

PAPER • OPEN ACCESS

Topological pumping in acoustic waveguide arrays with hopping modulation

To cite this article: Zhaoxian Chen *et al* 2022 *New J. Phys.* **24** 013004

New Journal of Physics
The open access journal at the forefront of physics

Deutsche Physikalische Gesellschaft DPG
IOP Institute of Physics

Published in partnership with: Deutsche Physikalische Gesellschaft and the Institute of Physics

OPEN ACCESS

RECEIVED
13 July 2021

REVISED
23 November 2021

ACCEPTED FOR PUBLICATION
30 November 2021

PUBLISHED
30 December 2021

PAPER

Topological pumping in acoustic waveguide arrays with hopping modulation

Zhaoxian Chen[1,2], Zeguo Chen[3], Zhengwei Li[1], Bin Liang[1,*], Guancong Ma[3], Yanqing Lu[2] and Jianchun Cheng[1]

[1] Key Laboratory of Modern Acoustics, MOE, Institute of Acoustics, Department of Physics, Collaborative Innovation Center of Advanced Microstructures, Nanjing University, Nanjing 210093, People's Republic of China
[2] College of Engineering and Applied Sciences, Nanjing University, Nanjing 210093, People's Republic of China
[3] Department of Physics, Hong Kong Baptist University, Kowloon Tong, Hong Kong, People's Republic of China
[*] Author to whom any correspondence should be addressed.

E-mail: liangbin@nju.edu.cn

Keywords: topological acoustics, edge state pumping, hopping modulation

Abstract

Thouless pumping is the adiabatic transportation of quantized charge, which is regarded as the dynamic version of the quantum Hall effect. Here we propose the design of an acoustic system to demonstrate the topological pumping characterized by transporting acoustic energy from one side to the opposite. The system is composed of coupled acoustic waveguide arrays with modulated coupling along both cross-sections and the propagating direction. We explore multiple topological phases by introducing rich spatial frequency or enlarged range of the hopping modulation. Such distinct topological phases are evidenced by adiabatic evolution of the edge states, where the acoustic system varies continuously and slowly along the state propagating direction. The robustness behavior of the edge states transport is also verified with numerical simulations to imply their topology origin. Our work provides a route to realize topological phases and utilize the corresponding edge states in waveguide arrays that can lead to versatile acoustic wave manipulation applications.

1. Introduction

Topology provides additional insights and freedom to understand the phase of matter, which paves new ways to manipulate electrons [1, 2], photons [3, 4] and phonons [5, 6]. A notable topology phase is the Chern insulator that breaks time-reversal symmetry and has one-way propagating states along the edges. Electromagnetic-wave systems are a great platform for realizing Chern insulators [7–9]. In contrast, however, magneto-acoustic effects are usually too weak to realize nonreciprocal acoustic wave propagation with a magnetic field. To overcome this obstacle, it is theoretically proposed that biased angular momentum by allowing a moving medium can break the time-reversal symmetry for sound and enables acoustic Chern insulators [10–13], which have been experimentally demonstrated [14]. However, it is quite challenging to control the airflow in complicated systems and the active components, such as rotating motors. Such strategies are also energy-consuming.

Another prominent manifestation of band topology is through the Thouless pumping, which originally refers to the quantized charge transportation in electrons systems with adiabatic and cyclic parameter variation [15, 16]. In classical-wave systems, Thouless pumping is about the adiabatic evolution and transportation of the edge states and can be used to characterize the topological invariants [17–21]. In acoustics, however, dissipations and active modulations have been the obstacles preventing the realization of pumping in time domain. Recently, a successful temporal acoustic pumping of topological modes was reported using a bilayer aperiodic acoustic lattice [22]. On the other hand, the time-dependent Schrödinger equation and the paraxial wave equation share a similar mathematical form. This fact has been leveraged for the realization of Thouless pumping by mapping the temporal evolution to the spatial dimension along the

propagative direction [18, 19, 23–31]. Very recently, both onsite [23] and hopping [31] modulation strategies have been developed in acoustic waveguide systems to explore the propagating effects of topological edge states. However, how to fully design different hopping effects to realize distinct topological phases is still an open question.

Here, we use an acoustic waveguide array as a platform to explore the topological phases and implement topological pumping in real spaces by introducing parameter evolution along the propagating direction. The coupling can be modulated freely without affecting the onsite potential, so the cross-sections of the waveguide array reproduce commensurate hopping modulating Harper models. Harnessing the dipole-like mode profile of the first-order guiding mode, we design both positive and negative coupling effects simultaneously and realize a novel trimeric Harper model, where the gap Chern numbers are ± 2. The energy spectra and mode distributions are thoroughly investigated with the finite element methods (FEM) and the tight-binding models (TBMs). We enforce adiabatic variations along the propagating direction by changing the positions of the coupling channels and numerically realize topological pumping that acoustic energy transfers from one side to the opposite of the array. Our system shows excellent robustness, which is of great importance for topological phase design and wave manipulation.

2. Models and results

2.1. Positive and negative hopping coefficients

The schematic of the proposed acoustic waveguide array with coupling modulated along the propagating direction is shown in figure 1(a). The waveguides have geometric parameters $h = 20$ mm and $w = 4$ mm, and they are connected by two narrow channels with thickness $h_c = 2$ mm. The total length of the short (long) channels is $l_n = 10$ mm ($l_p = 30$ mm), which is optimized to provide negative (positive) hopping [32]. All the waveguides and coupling components are filled with air with density $\rho = 1.21$ kg m^{-3} and sound speed $c = 340$ m s^{-1}. For one single waveguide, its first-order guiding mode has a cut-off of $f_0 = 8550$ Hz. This mode has a dipole-like cross-sectional profile with one nodal plane at the center and two anti-nodes with opposite phases at the two ends. The coupling strength is therefore tunable by changing u_n and u_p, which are the positions of the coupling channels. Using the FEM software COMSOL Multiphysics, we first study the case of a two-cavity coupling system with a short channel and get the eigenfrequencies as a function of u_n, as marked by the black dots in figure 1(b). When the short channel moves towards the end of the cavity, the two eigenfrequencies split almost linearly around f_0, which means the coupling strength increases monotonously with $|u_n|$ but with negligible effect on the onsite potential. Insets show the pressure fields in the two cavities which are in-phase for the lower frequency mode but out-of-phase for the higher frequency mode, indicating a negative coupling effect. As a result, we can use a TBM to fit this two-cavity system with a two-element Hamiltonian $\mathbf{H} = [f_0, t; t, f_0]$, in which $t \in \mathrm{R}$ represents the hopping coefficient. The eigenfrequencies are plotted as functions of u_n in figure 1(b). From the splitting of the eigenfrequencies we can also extract the hopping t, which clearly has a one-to-one correspondence to u_n. When the short coupling channel is replaced with a long one, as shown in figure 1(c), it is easy to find that there is still a good linear relationship between $|u_p|$ and t. Comparing figures 1(b) and (c), the parities of the lower and higher modes are flipped, which indicates different signs of the hopping coefficient. From the modal parities, it can be inferred that the short coupling channel introduces negative hopping, with even mode at a lower frequency, whereas the long channel introduces positive hopping, for which the lower mode is an odd mode. Compared with other designs of hopping modulation [31, 33], the advantage here is that the hopping can be freely tailored without affecting the onsite potential. As a result, we can easily design both the strength and the sign of the coupling by using the two channels simultaneously.

2.2. Topological phase diagram of Harper models with $\beta = 1/3$

Before designing different topology system with the coupling strategies discussed above, we study the topological properties of a hopping modulating commensurate Harper model with the Hamiltonian of the TBM expressed as [34]

$$\hat{\boldsymbol{H}}(\varphi) = \sum_{j=1}^{N} f_0 c_j^{\dagger} c_j + \sum_{j=1}^{N-1} [t_{j,j+1}(\varphi)\, c_j^{\dagger} c_{j+1} + \mathrm{H.c.}], \tag{1}$$

where N is the total number of the on-site elements with potential f_0, j denotes the site indexes, $c_j^{\dagger}$ and c_j are respectively the creation and annihilation operators of the jth site. The hopping coefficient follows a cosine modulation

$$t_{j,j+1}(\varphi) = t_0 + t_m \cos(2\pi\beta j + \varphi), \tag{2}$$

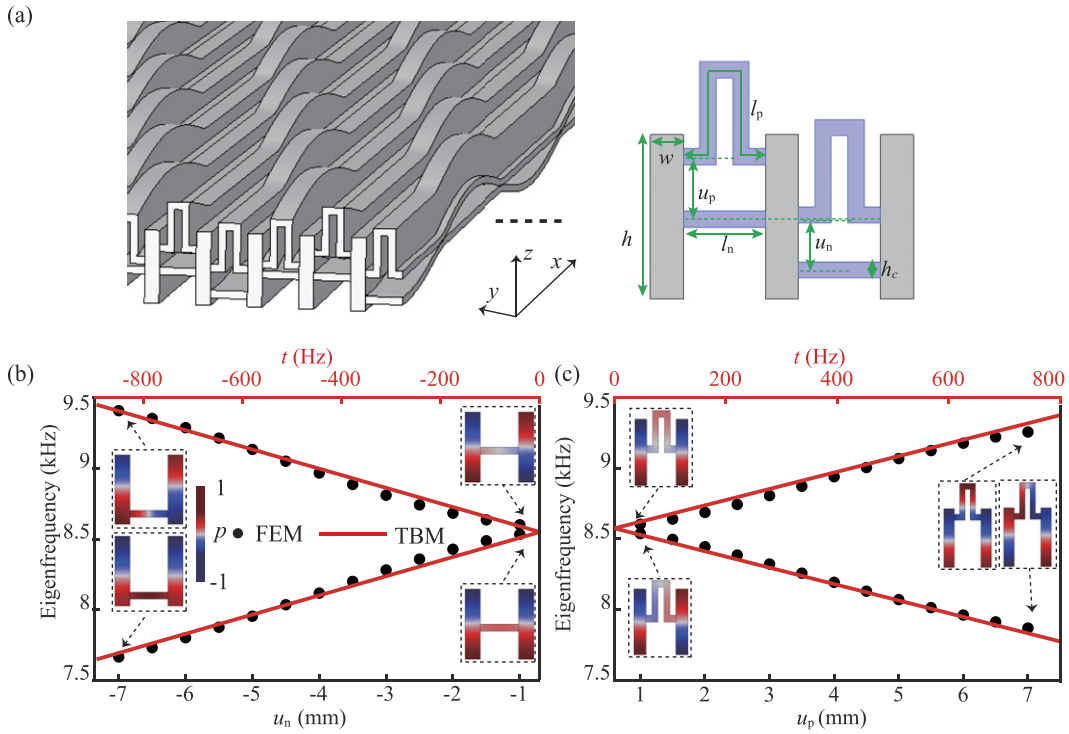

Figure 1. (a) Schematic of an acoustic waveguide array with the coupling modulating along the propagating direction. The short and long channels contribute to negative and positive coupling, respectively. The cross-section of the array reproduces a hopping modulating commensurate Harper model. The right panel labels geometry parameters which are set as $h = 20$ mm, $w = 4$ mm, $l_n = 10$ mm, $l_p = 30$ mm and $h_c = 2$ mm, respectively. Here u_p and u_n are the positions of the coupling channels along the z direction, and the waveguides are centered at $z = 0$. (b) Eigenfrequencies of the two-cavity system with short coupling channel obtained from the FEM simulations as a function of u_n (black dots) and TBM calculations as a function of t (red curves), respectively. Insets: eigenmodes for $u_n = -7$ and -1 mm, respectively. (c) Eigenfrequencies of the two-cavity system with long coupling channel.

where φ is the initial modulating phase, t_0 and t_m are respectively the static coupling effect and modulating strength, β is the spatial modulating frequency. For the case of $\beta = 1/3$, the unit cell of this hopping modulating Harper model consists of three elements and its Hamiltonian is expressed as

$$\mathbf{H}\left(\varphi, k_y\right) = \begin{bmatrix} f_0 & t_{1,2}\left(\varphi\right) & t_{3,4}\left(\varphi\right) \mathrm{e}^{-\mathrm{i}k_y} \\ t_{1,2}\left(\varphi\right) & f_0 & t_{2,3}\left(\varphi\right) \\ t_{3,4}\left(\varphi\right) \mathrm{e}^{\mathrm{i}k_y} & t_{2,3}\left(\varphi\right) & f_0 \end{bmatrix}, \tag{3}$$

which represents an effective 2D system in the synthetic k_y-φ space. The Chern number of the nth band is defined as [35, 36]

$$C_n = \frac{1}{2\pi} \int_{-\pi}^{\pi} \mathrm{d}k_y \int_0^{2\pi} \mathrm{d}\varphi F_n(k_y, \varphi), \tag{4}$$

where $F_n\left(k_y, \varphi\right) = \langle \psi_n | \nabla_{k_y,\varphi} | \psi_n \rangle$ is the Berry curvature. The topological invariants for the gaps are gap Chern numbers, which are the summation of the band Chern numbers below them [37]. When the onsite potentials of the Harper model are identical, the energy spectra shall be mirror symmetric about the zero energy and the topological phases are determined by the relation between t_0 and t_m. We define energy gap G as

$$G = \min_{\varphi,k_y}(E^2_{\varphi,k_y} - E^1_{\varphi,k_y}), \tag{5}$$

where E^1_{φ,k_y} and E^2_{φ,k_y} are the first and second band over the Brillouin zone. Figure 2 shows the energy gap G as a function of t_m/t_0 and the figure is divided into three parts according to their topological features. For the region of $|t_m/t_0| < 4$, where the hopping modulation t_m is relatively weak compared with t_0, the gap Chern numbers are $(-1, 1)$. For region of $|t_m/t_0| > 4$ with sufficiently strong hopping modulation t_m, the system is in a distinct topological phase with large gap Chern numbers $(2, -2)$ and the energy gap G increases monotonously with $|t_m/t_0|$. The extreme case is $t_0 = 0$ where the hopping $t_{j,j+1}\left(\varphi\right)$ just modulates around 0 and the system will have the maximum global band gap $G = 0.65t_m$. For the phase transition points of $|t_m/t_0| = 4$, the two energy gaps close and the topological invariants are not well defined. As a

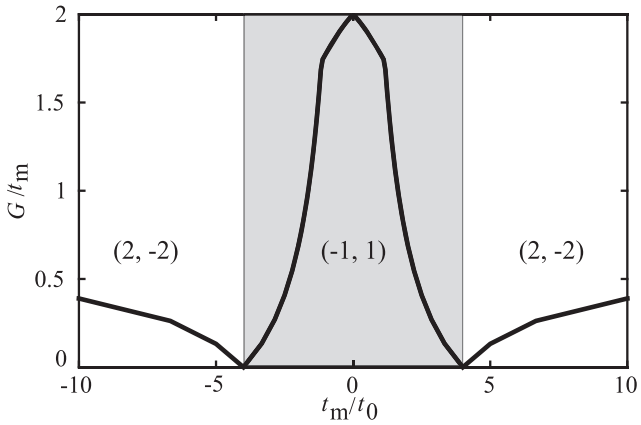

Figure 2. Phase diagram for the hopping modulating Harper model with $\beta = 1/3$. The black curve delineates the size of the energy gap G as a function of t_m/t_0. Gap Chern numbers are indicated in the parentheses.

result, figure 2 gives clear guidance for designing and selecting the topological feature of the Harper model with $\beta = 1/3$.

2.3. Topological pumping with gap Chern number of 2

To get Chern numbers larger than one in a trimeric hopping modulating Harper model, according to the topological phase diagram in figure 2, the hopping should be designed within a quite large range covering both negative and positive values. Thus, as shown in figure 1(a), both short and long channels are employed to design the coupling coefficients. We set the center of the waveguides to be $z = 0$ and the positions of the coupling channels are modulated by

$$u^{n}_{j,j+1}(\varphi) = u^{n}_{m}[\cos(2\pi j/3 + \varphi) < 0], \tag{6a}$$

$$u^{p}_{j,j+1}(\varphi) = u^{p}_{m}[\cos(2\pi j/3 + \varphi) > 0], \tag{6b}$$

where u^{n}_{m} and u^{p}_{m} are the modulating amplitudes for short and long coupling channels, respectively. There are two channels between every two waveguides, according to equation (6) and their positions change alternatively so that one of the channels always stays at the center of the waveguide with no coupling contribution. We choose $u^{n}_{m} = 6$ mm and $u^{p}_{m} = 7$ mm so that both the positive and negative couplings share the same modulating amplitudes. As a result, the cross-section of the whole waveguide array reproduces a commensurate Harper model with hopping modulating as

$$t_{j,j+1}(\varphi) = 0 + 0.1f_0\cos(2\pi j/3 + \varphi). \tag{7}$$

Using both the FEM simulations and the TBMs calculations, we get the energy spectra of the array's cross-section with $N = 14$ and the results as a function of φ are shown in figures 3(a) and (b). The spectra match well, meaning that the waveguide array's cross section can be effectively fitted by a TBM. The band structures both have 3 groups of bulk bands separated by two gaps which are bridged by topological boundary states (TBSs). We also note the energy spectra are almost mirror symmetric about f_0 due to the chiral symmetry [38]. Here we have $|t_m/t_0| = \infty$, so the gap Chern numbers are $I_1 = 2$ and $I_2 = -2$, respectively, which are labeled in figure 3(b). According to the bulk-edge correspondence, every side of the system has two TBSs [18, 39, 40]. For φ varying from $-\pi$ to π, the TBSs in the gaps can transfer from the left to the right side of the system twice, which is clearly illustrated with the mode field distributions and eigenfunctions in figures 3(c) and (d). Due to the presence of both the positive and negative hopping effect, the energy gap is large as $0.065f_0$, and the TBSs are very robust against disorders, which will be demonstrated with the topological pumping process. Note that the details of the TBSs depend on the boundary types. In our system, the total number of the waveguides N contributes to additional freedom to design the configurations of the TBSs [23]. In addition, there are infinite bands in our acoustic coupling system, and the higher frequency gaps may exhibit higher Chern numbers. However, these bands are usually messy and the gaps are too small to support well-localized edge states. This might be the reason why the gaps with higher Chern numbers are less researched [3–6]. However, higher gap Chern numbers mean more TBSs in the gaps, which are beneficial for designing multimode waveguides [39, 40]. As a result, in this work, we mainly explore the topological systems with higher gap Chern numbers to showcase the advantage of our hopping design strategy.

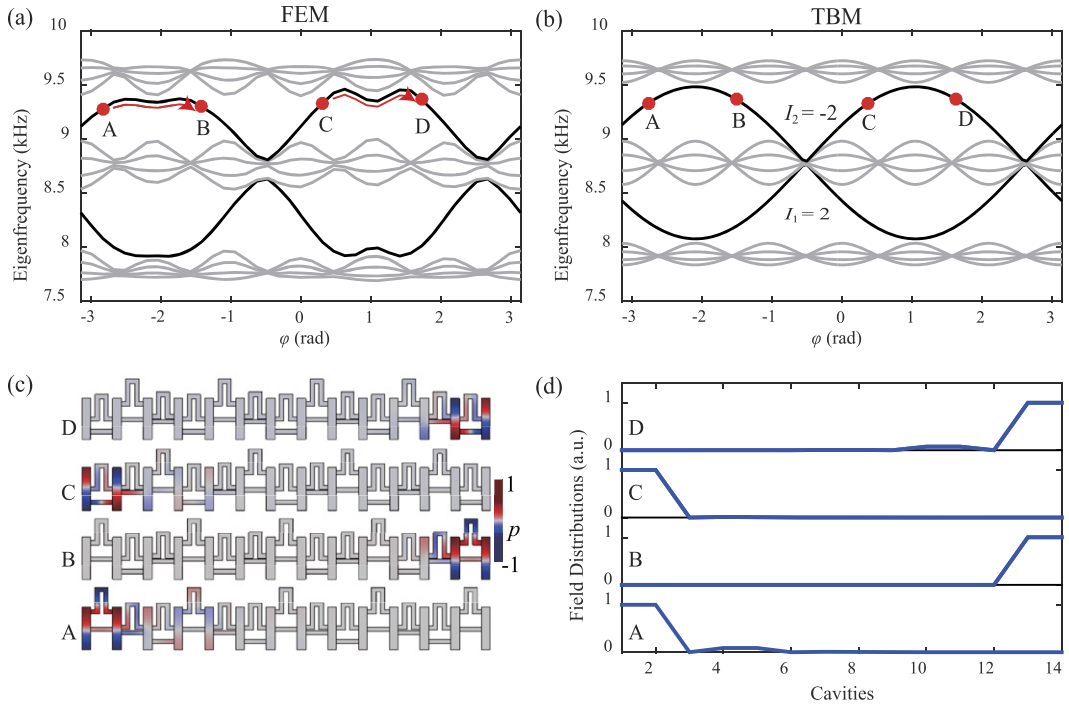

Figure 3. (a) Energy spectra obtained by FEM simulation of the waveguide array's cross-section as a function of φ and (b) by solving the TBM Hamiltonian with open boundaries. Gray curves are bulk states and black curves are TBSs. Red arrow curves denote the pumping processes. (c) Mode field distributions and (d) eigenfunctions for the cases labeled in (a) and (b), respectively.

Considering the wave propagations in such a waveguide array, the first-order guiding mode can be described as $|\psi_n(\varphi)\rangle e^{ik_x x}$, where $|\psi_n(\varphi)\rangle$ is the mode field distributions of the nth eigenfrequency $f_{\mathrm{H},n}(\varphi)$. When we set the working frequency as f_{w}, the propagating constant can be calculated as $k_{x,n}(\varphi) = 2\pi/c\sqrt{f_{\mathrm{w}}^2 - f_{\mathrm{H},n}^2(\varphi)}$ [41] where c is the sound speed of the medium. Since the wave dynamics in such waveguide array is determined by φ, as schematically shown in figure 1(a), we enforce the adiabatic variation of φ in the waveguide array by slowly modulating the coupling channels along the propagating x direction such that φ is linearly linked with x. Then the wave propagation can be described as

$$-\mathrm{i}\partial_x|\psi(x)\rangle = H(x)|\psi(x)\rangle. \tag{8}$$

Notice that this equation is mathematically similar to Schrödinger equation with temporal derivative replaced by spatial derivative.

Now we revisit the eigenvalues in figure 3(a) and study the pumping process of the TBS in the upper bandgap. When φ varies from $-\pi$ to $-\pi$, this TBS transfers from the left side (marked as A and C) to the right side (B and D) of the system twice. In the 3D waveguide system (figure 1(a)), the acoustic energy should be pumped from one side to the opposite side by slowly modulating the hopping along the propagating direction. For a practical implementation, we set the length of the array as $L = 1$ m and the positions of the coupling channels follow equation (6) with φ varying continuously from $\varphi_{\mathrm{A}} = -0.8\pi$ to $\varphi_{\mathrm{B}} = -0.5\pi$. When we put an acoustic dipole source of 9500 Hz at the left side of the array, as shown in figure 3(a), the acoustic wave follows the adiabatic evolution and emerges into the bulk firstly and lets out from the right side finally. The inset shows the pumping ratio which is defined as energy in the rightmost two waveguides over all the energy at the output for the case from A to B. When $L > 0.5$ m, the adiabatic condition is well satisfied and most of the energy is pumped to the right side. Here we also provide the corresponding mode areas S_{m} of the TBS and bulk states. S_{m} quantitatively shows the localization of the eigenmode for the array's cross-section [42, 43] and is defined as:

$$S_{\mathrm{m}}(\varphi) = \frac{\iint |p(\mathbf{r},\varphi)|^2 \mathrm{d}\mathbf{r}}{\max\{|p(\mathbf{r},\varphi)|^2\}}, \tag{9}$$

where $\mathbf{r}$ represents all the area of the cross-section. For TBSs in which acoustic energy is mainly localized at the boundaries, their S_{m} should be small as compared to bulk states for which energy is dispersed across the system. For the process of A to B, as shown in figure 4(b), the TBS's mode area S_{m} increases first and then

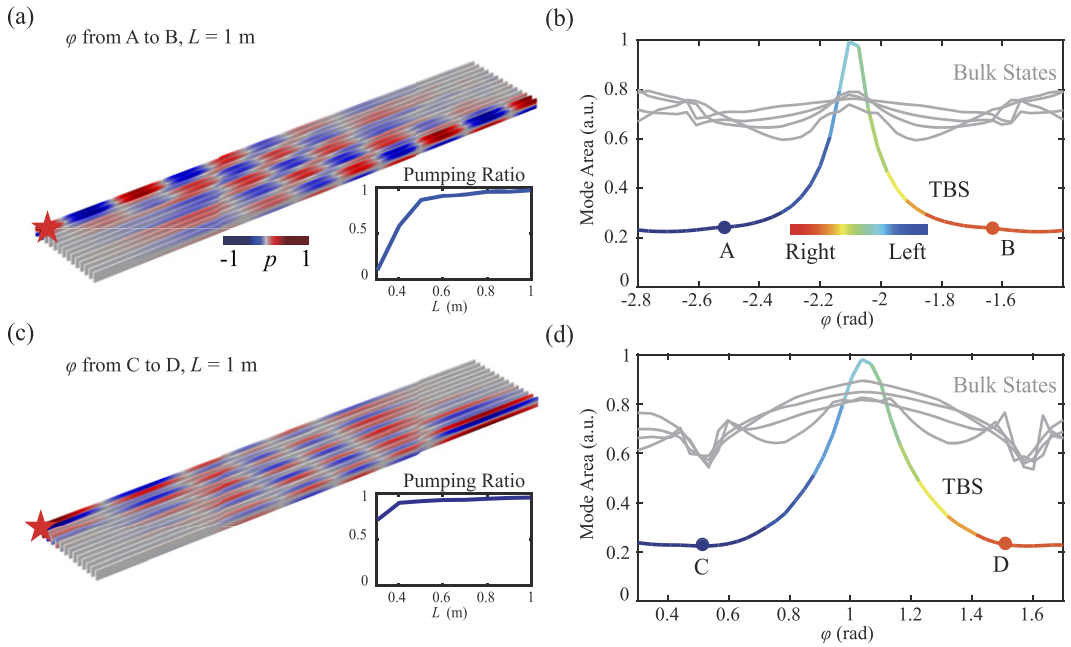

Figure 4. (a) Simulated pumping process of waveguide arrays with a length $L = 1$ m and φ varying from $\varphi_A = -0.8\pi$ to $\varphi_B = -0.5\pi$. The red star marks the exciting source location with $f_w = 9500$ Hz and inset shows the pumping ratio with L. (b) Mode areas of the corresponding TBS and bulk modes. Pseudo colors from blue to red are used to visualize the weightings of the left and right TBSs. (c) The pumping process for C to D with φ varying from $\varphi_C = 0.15\pi$ to $\varphi_D = 0.45\pi$ and (d) the corresponding mode areas.

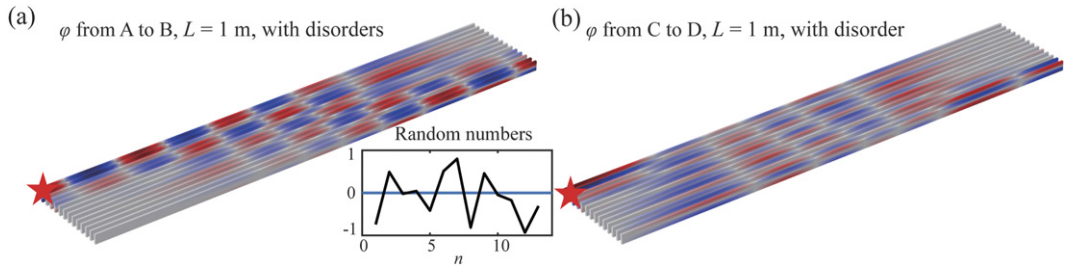

Figure 5. Robustness analysis of the pumping process of (a) A to B and (b) C to D. The inset shows the random numbers for the perturbation function. Other parameters are the same as in figure 4.

decreases. Its localization property is also marked in different colors, which indicates the TBS transfers continuously from the left side to the right side via some bulk states and is consistent with the field distributions in figure 4(a). For the process of C to D, in which φ varies from $\varphi_C = 0.15\pi$ to $\varphi_D = 0.45\pi$, the TBS also transfers from the left to the right side and there is an up-and-down process for its mode area, which is clearly shown in figure 4(d). As a result, as shown in figure 4(c) and the inset, adiabatic condition can also be well satisfied when $L > 0.4$ m and the acoustic energy will be pumped from the left to the right side of the array. However, for the processes of B to C or D to A, the TBSs are very close to the bulk states. Therefore, much longer waveguides are needed for the adiabatic condition to be well satisfied.

To demonstrate the strong robustness of our system against defects, here we introduce disorders to the system in the form of random perturbations for the coupling channels' positions along the z direction. The perturbation function is give as $\delta u = s u_m R_{(-1,1)}$, where $s = 0.1$ is the perturbation strength, $u_m = 6.5$ mm is the average modulation amplitude for the channels and $R_{(-1,1)}$ is a random number within $(-1, 1)$. As shown in figure 5, both the pumping processes are well preserved under such large disorders. We note the strong robustness is guaranteed by the large gap, which is attributed to the introduction of both the positive and negative hopping effects.

2.4. Topological pumping with $\beta = 1/5$

Since Harper models are connected to the two-dimensional Hofstadter spectrum of the integer quantum Hall effect [44], instead of designing both positive and negative hopping effects simultaneously, we can

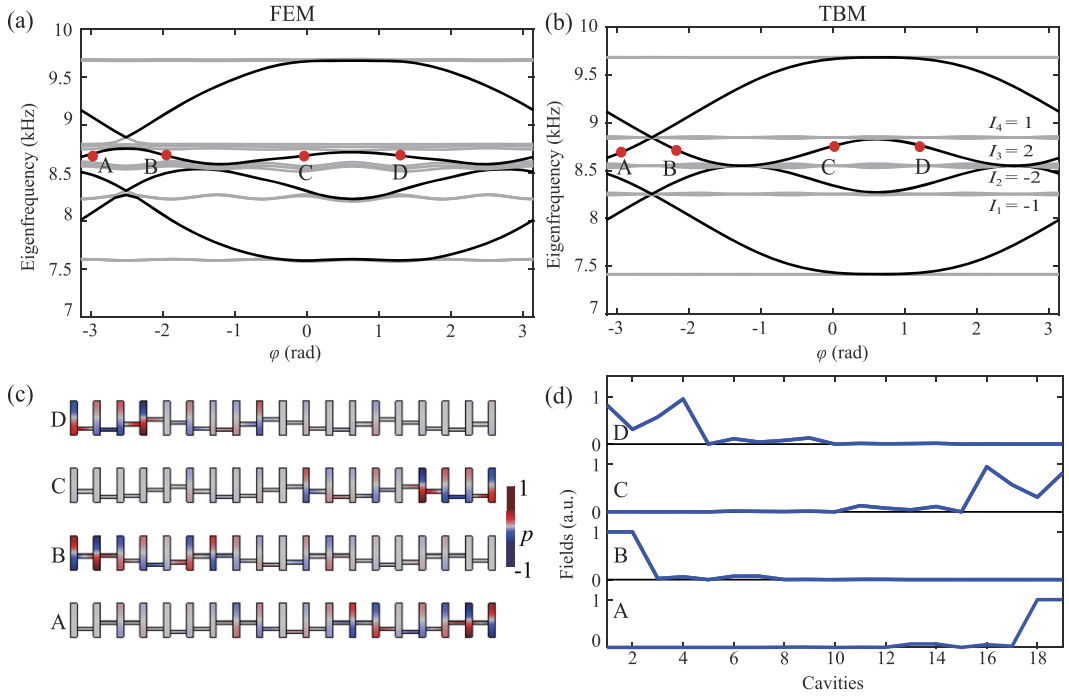

Figure 6. (a) Energy spectra obtained by FEM simulation of the waveguide array's cross-section as a function of φ. There is only one short coupling channel between every two waveguides, and the channel position follows equation (10), where we set $\beta = 1/5$, $N = 19$, $u_0 = -4$ mm and $u_m = 3$ mm. Other parameters are the same as in figure 1. (b) Energy spectra obtained by solving the Hamiltonian of the Harper models with hopping modulated as equation (11). (c) Mode field distributions and (d) eigenfunctions for the cases labeled in (a) and (b), respectively.

change the spatial modulating frequency β to get gaps with higher Chern numbers (the Hofstadter spectra are provided in the appendix). For example, there are gaps with Chern numbers of ± 2 when we set $\beta = 1/5$. However, we find the gaps of this topological phase are small, thus the system is not robust enough for topological pumping behaviors. For demonstration, here we only use the short channels for the hopping design and modulate their positions as

$$u_{j,j+1}(\varphi) = -u_0 + u_m \cos(2\pi j/5 + \varphi). \tag{10}$$

According to the coupling analysis shown in figure 1(b), we set $u_0 = -4$ mm and $u_m = 3$ mm so that the cross-section of the whole waveguide array reproduces a commensurate Harper model with hopping modulated as

$$t_{j,j+1}(\varphi) = -0.05f_0 + 0.05f_0 \cos(2\pi j/5 + \varphi). \tag{11}$$

With these parameters, a system with $N = 19$ is analyzed and the spectra for the FEM simulations and TBM calculations are shown in figures 6(a) and (b), respectively. As labeled in figure 6(b), the central two gaps are with Chern numbers of $I_2 = -2$ and $I_3 = 2$, respectively. However, because the hopping modulation amplitude reduces by half but the gap number doubles, here the two gaps are much smaller and are only about one-third of the gaps in figures 3(a) and (b). As a result, the TBSs, whose profiles are shown in figures 6(c) and (d), are not well localized at the boundaries, and the robustness of the system is not strong.

Now we numerically study the topological pumping processes in this waveguide system, where the channels' positions are continuously modulated along the propagating direction following equation (10). For the process of A to B, in which φ of the waveguide array varies from $\varphi_A = -0.95\pi$ to $\varphi_B = -0.65\pi$, we use $f_w = 8800$ Hz as the working frequency to excite the TBS in the third bandgap. As shown in figure 7(a), the acoustic energy cannot be completely pumped to the opposite side of the array even when we set the waveguide length $L = 2$ m. Considering the poor localization of the TBSs, here the pumping ratio is defined as the energy in the rightmost four waveguides over all the energy at the output. Comparatively, the pumping ratios in the inset are much lower than the cases in figure 4. To test the robustness of the system, we also introduce perturbations to the channels' positions and keep $s = 0.1$ for the perturbation function $\delta u = s u_m R_{(-1,1)}$. Though here the modulation amplitude u_m decreases to 3 mm, as shown in figure 7(b), the pumping process almost fails after introducing the disorders. According to figures 7(c) and (d), which are about the process of C to D with φ varying from $\varphi_C = 0.05\pi$ to $\varphi_D = 0.35\pi$, we can get the same conclusion that the system is fragile and the pumping efficiency is relatively low. As a result, our strategy for

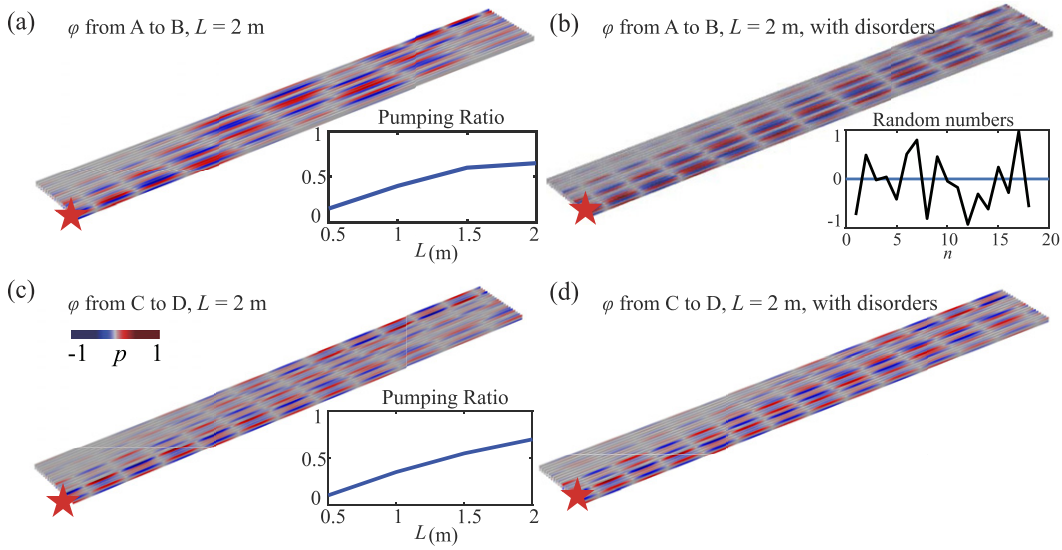

Figure 7. (a) Simulated pumping process in a waveguide array with length $L = 2$ m and φ varying from $\varphi_A = -0.95\pi$ to $\varphi_B = -0.65\pi$. The working frequency is $f_w = 8800$ Hz and the inset shows the pumping ratio with L. (b) The pumping process with disorders for the channel positions. The inset shows the random numbers for the perturbations. (c) and (d) The pumping process for C to D with φ varying from $\varphi_C = 0.05\pi$ to $\varphi_D = 0.35\pi$. The pumping processes are of low efficiency and fail with the introduction of disorders.

designing positive and negative hopping effects has great advantages for designing novel topological phases and implementing topological pumping with gap Chern numbers larger than one.

In addition, the hopping modulation strategy developed in this work also shows many advantages when compared with the modulation of onsite potentials [23]. First of all, since both the strength and sign of the hopping effect can be tailored freely, we have more freedom to design the topological phases. As proved in section 2.3, by introducing both the positive and negative hopping effects simultaneously, we can get enlarged gaps with Chern numbers of ± 2 when the spatial modulating frequency is $\beta = 1/3$. However, for onsite modulating Harper models with the same β, we can only get gap Chern numbers of ± 1 even we increase the modulation amplitude to a large unrealizable value. Secondly, the hopping modulation strategy in our acoustic waveguide system may have higher experimental feasibility for the topological pumping process. Specifically, our hopping modulation is applied to the positions of the coupling channels, which vary within half of the waveguide's height. By contrast, for the onsite potential modulation, the variables are the heights of the waveguides, which can only be modulated within a much smaller range for mapping a Harper model. In addition, the hopping modulation strategy is more applicable for showcasing the pumping process of higher-order topological states, such as the corner states [31].

3. Conclusion

To conclude, we propose a design of acoustic waveguide arrays whose cross-sections reproduce hopping modulating Harper models. By introducing both positive and negative coupling effects simultaneously, a distinct topological phase appears, and we can get topological gaps with larger sizes and higher Chern numbers simultaneously. With doubled hopping modulating amplitude, the edge states therein have strong robustness, which is guaranteed by the large gap sizes. With the hopping continuously modulated along the propagating direction to enforce adiabatic variations, topological pumping is numerically implemented as input acoustic energy transfers from one side of the array to the opposite. Our work provides an insight to the physics underlying the coupling effect and offers new possibilities for manipulating acoustic waves and other classical waves, with far-reaching impact in acoustic and many related fields.

Acknowledgments

This work was supported by National Key R & D Program of China (Grant No. 2017YFA0303700), the National Natural Science Foundation of China (Grant Nos. 11634006, 11374157, 81127901, 11802256, 11922416), a project funded by the Priority Academic Program Development of Jiangsu Higher Education

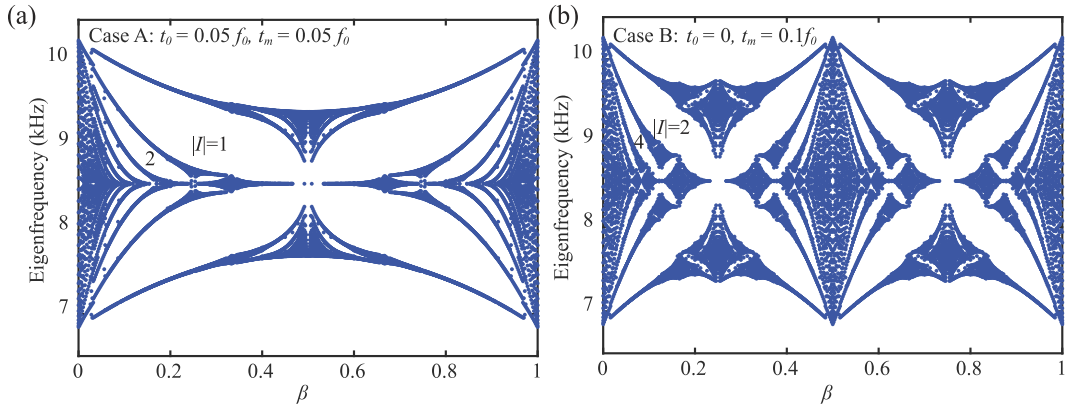

Figure A1. Hofstadter spectra for the hopping modulating Harper models (a) with regular hopping modulation and (b) with both positive and negative hopping modulations. Chern numbers are labeled in the gaps.

Institutions and High-Performance Computing Center of Collaborative Innovation Center of Advanced Microstructures.

Data availability statement

The data generated and/or analysed during the current study are not publicly available for legal/ethical reasons but are available from the corresponding author on reasonable request.

Appendix. Hofstadter energy spectrum

In this appendix, we analyze the hopping modulating Harper models with the Hofstadter energy spectrum, which clearly present the fractal structure of the topological gaps. For the hopping effect in equation (2) that $t_{j,j+1} = t_0 + t_m \cos(2\pi\beta j)$, we define case A with $t_0 = 0.05f_0$ and $t_m = 0.05f_0$, which refers to the regular coupling modulation, and define case B with $t_0 = 0$ and $t_m = 0.1f_0$, where both the positive and negative coupling effects are involved. When β samples rational values from 0 to 1, we get the corresponding Hofstadter butterfly spectra, which are shown in figure A1.

For case A with regular hopping modulation, the largest gaps are with Chern numbers of $|I| = 1$. There are gaps with higher Chern numbers, but their sizes are much smaller. By contrast, when both positive and negative hopping effects are involved in case B, the largest gaps have $|I| = 2$. In addition, except $\beta = 0.5$, the spectrum is also symmetric about $\beta = 0.25$ and $\beta = 0.75$, which can be attributed to the zero-centered hopping modulation function. As a result, mixing positive and negative coupling effects is an effective way to increase the hopping modulation amplitude and to realize wide gaps with distinct topological features.

ORCID iDs

Bin Liang https://orcid.org/0000-0003-2655-9024

References

[1] Qi X-L and Zhang S-C 2011 *Rev. Mod. Phys.* **83** 1057
[2] Hasan M Z and Kane C L 2010 *Rev. Mod. Phys.* **82** 3045
[3] Lu L, Joannopoulos J D and Soljačić M 2014 *Nat. Photon.* **8** 821
[4] Ozawa T *et al* 2019 *Rev. Mod. Phys.* **91** 015006
[5] Ma G, Xiao M and Chan C T 2019 *Nat. Rev. Phys.* **1** 281
[6] Zhang X, Xiao M, Cheng Y, Lu M-H and Christensen J 2018 *Commun. Phys.* **1** 97
[7] Wang Z, Chong Y D, Joannopoulos J D and Soljačić M 2008 *Phys. Rev. Lett.* **100** 013905
[8] Wang Z, Chong Y, Joannopoulos J D and Soljačić M 2009 *Nature* **461** 772
[9] Poo Y, Wu R-X, Lin Z, Yang Y and Chan C T 2011 *Phys. Rev. Lett.* **106** 093903
[10] Fleury R, Sounas D L, Sieck C F, Haberman M R and Alù A 2014 *Science* **343** 516
[11] Khanikaev A B, Fleury R, Mousavi S H and Alù A 2015 *Nat. Commun.* **6** 8260
[12] Ni X, He C, Sun X-C, Liu X-P, Lu M-H, Feng L and Chen Y-F 2015 *New J. Phys.* **17** 053016
[13] Yang Z, Gao F, Shi X, Lin X, Gao Z, Chong Y and Zhang B 2015 *Phys. Rev. Lett.* **114** 114301
[14] Ding Y, Peng Y, Zhu Y, Fan X, Yang J, Liang B, Zhu X, Wan X and Cheng J 2019 *Phys. Rev. Lett.* **122** 014302

[15] Thouless D J 1983 *Phys. Rev.* B **27** 6083
[16] Nakajima S, Tomita T, Taie S, Ichinose T, Ozawa H, Wang L, Troyer M and Takahashi Y 2016 *Nat. Phys.* **12** 296
[17] Lohse M, Schweizer C, Zilberberg O, Aidelsburger M and Bloch I 2016 *Nat. Phys.* **12** 350
[18] Ke Y, Qin X, Mei F, Zhong H, Kivshar Y S and Lee C 2016 *Laser Photon. Rev.* **10** 995
[19] Long Y and Ren J 2019 *J. Acoust. Soc. Am.* **146** 742
[20] Chen H, Yao L Y, Nassar H and Huang G L 2019 *Phys. Rev. Appl.* **11** 044029
[21] Shen Y-X, Zeng L-S, Geng Z-G, Zhao D-G, Peng Y-G and Zhu X-F 2020 *Phys. Rev. Appl.* **14** 014043
[22] Cheng W, Prodan E and Prodan C 2020 *Phys. Rev. Lett.* **125** 224301
[23] Chen Z-G, Tang W, Zhang R-Y, Chen Z and Ma G 2021 *Phys. Rev. Lett.* **126** 054301
[24] Shen Y X, Peng Y G, Zhao D G, Chen X C, Zhu J and Zhu X F 2019 *Phys. Rev. Lett.* **122** 094501
[25] Rosa M I N, Pal R K, Arruda J R F and Ruzzene M 2019 *Phys. Rev. Lett.* **123** 034301
[26] Kraus Y E, Lahini Y, Ringel Z, Verbin M and Zilberberg O 2012 *Phys. Rev. Lett.* **109** 106402
[27] Zilberberg O, Huang S, Guglielmon J, Wang M, Chen K P, Kraus Y E and Rechtsman M C 2018 *Nature* **553** 59
[28] Lustig E, Weimann S, Plotnik Y, Lumer Y, Bandres M A, Szameit A and Segev M 2019 *Nature* **567** 356
[29] Riva E, Casieri V, Resta F and Braghin F 2020 *Phys. Rev.* B **102** 014305
[30] Riva E, Rosa M I N and Ruzzene M 2020 *Phys. Rev.* B **101** 094307
[31] Chen H, Zhang H, Wu Q, Huang Y, Nguyen H, Prodan E, Zhou X and Huang G 2021 *Nat. Commun.* **12** 5028
[32] Chen Z-G, Wang L, Zhang G and Ma G 2020 *Phys. Rev. Appl.* **14** 024023
[33] Qi Y, Qiu C, Xiao M, He H, Ke M and Liu Z 2020 *Phys. Rev. Lett.* **124** 206601
[34] Harper P G 1955 *Proc. Phys. Soc.* A **68** 879
[35] Fukui T, Hatsugai Y and Suzuki H 2005 *J. Phys. Soc. Japan* **74** 1674
[36] Wang H-X, Guo G-Y and Jiang J-H 2019 *New J. Phys.* **21** 093029
[37] Hatsugai Y 1993 *Phys. Rev. Lett.* **71** 3697
[38] Yang Z-Z, Li X, Peng Y-Y, Zou X-Y and Cheng J-C 2020 *Phys. Rev. Lett.* **125** 255502
[39] Skirlo S A, Lu L and Soljačić M 2014 *Phys. Rev. Lett.* **113** 113904
[40] Skirlo S A, Lu L, Igarashi Y, Yan Q, Joannopoulos J and Soljačić M 2015 *Phys. Rev. Lett.* **115** 253901
[41] Blackstock D 2000 *Fundamentals of Physical Acoustics* (New York: Wiley)
[42] Oulton R F, Sorger V J, Genov D A, Pile D F P and Zhang X 2008 *Nat. Photon.* **2** 496
[43] Chen Z-X, Wu Z-J, Ming Y, Zhang X-J and Lu Y-Q 2014 *AIP Adv.* **4** 017103
[44] Hofstadter D R 1976 *Phys. Rev.* B **14** 2239